Effect of Resonance Frequency Mismatch for Transmission Power in Wireless Power Transfer System

Helanka Weerasekara
Graduate School of Engineering
The University of Tokyo
weerasekara.helanka18@ae.k.u-tokyo.ac.jp

Katsuhiro Hata
Institute of Industrial Science
The University of Tokyo

Takehiro Imura
Department of Electrical Engineering
Tokyo University of Science

Yoichi Hori
Department of Advanced Energy, Graduate School of Frontier Sciences
The University of Tokyo

***Abstract*—Wireless Power Transfer (WPT) for Electric Vehicles (EV) is one of an admirable solution to some obstacles of charging EVs. The operation frequency, secondary resonance frequency and primary resonance frequency are assumed to be equal in the previous WPT studies. In WPT, when primary and secondary side have different resonance frequencies due to inductance and capacitance change, it is called resonance frequency mismatch condition. This paper is investigated on the transmission power for the wireless power transfer systems with resonance frequency mismatch. The effectiveness of the theoretical analysis has been verified under resonance frequency mismatch condition by experimentally.**

***Index Terms*—Wireless power transfer, resonance frequency mismatch, transmission power**

I. Introduction

Electric Vehicle (EV) is well known as the new choice for vehicles in the future as it reduces CO2 emission and a great step forward in order with the growing concern for environmental issues around the world. Therefore, the EV appears to be one of the best options for public transportation and has raised the propagation of EV in the market. However, the common power source in EV, Li-ion battery is not able to provide energy as much as gasoline does. Therefore, EV can perform only short-distance cruising with one charge and have some problems of long charging time, many studies are performed on the in-motion wireless power transfer (WPT) of EV [1]– [6]. In WPT system, previous studies have been conducted assuming the primary side resonance frequency, the secondary side resonance frequency, and the operation frequency are same, to gain the maximum transmission efficiency [7]– [12].

However, in practice, the resonance frequency mismatch occurs when the inductance of the coil and capacitance of the capacitor changes, due to manufacturing errors, climate change and temperature variation. For instance, temperature variation affects the coil elasticity and the initial inductance of the coil will be changed. Therefore, the resonance frequency condition, mentioned above, can not be always applied for the WPT system. Using high quality coils and capacitors with less errors is one of the solutions to avoid the resonance frequency mismatch condition. Still, these solutions also have problems, such as high cost, sorting man-hours and some principle matters, thus it is necessary to analyze the WPT circuit with resonance frequency mismatch, to solve the parameter variation problem.

The transmission characteristics of various WPT systems can be mainly decided by the relationship between the source frequency and resonance frequency [13]– [14]. This paper is explored the influence of source frequency, primary and secondary side resonance frequency to transmission power by theoretically, and confirmed by experimentally. Power transmission is the movement of energy from input to a location where it is applied to perform useful work as output. The WPT circuit was first simulated to analyze the input power and then, simulations are done to investigate on output power by theoretically. Finally, the theoretical analyzing method for resonance frequency mismatch is confirmed at different resonance frequencies by experimentally.

II. WPT circuit analysis on transmission efficiency

In WPT system, the power is transferred from the transmitting coil to the receiving coil by inducing the voltage in receiving coil from magnetic field generation in transmitting coil.

In this paper, an SS-type WPT circuit is considered to analyze the WPT system with resonance frequency mismatch as shown in Fig. 1. Primary resonance frequency f_1 is related with primary side capacitance C_1 and inductance L_1, and secondary resonance frequency f_2 is related with secondary side capacitance C_2 and inductance L_2, are defined as follows:

$$f_1 = \frac{1}{2\pi\sqrt{L_1 C_1}}, \tag{1}$$

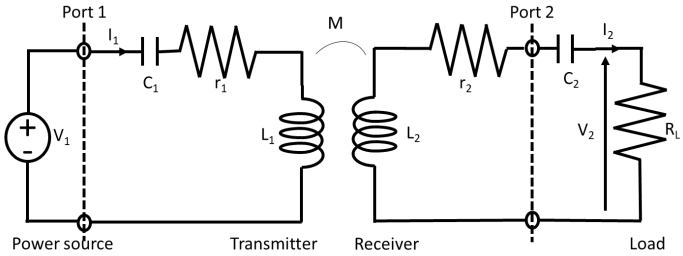

Fig. 1. Circuit diagram of SS type WPT circuit.

$$f_2 = \frac{1}{2\pi\sqrt{L_2C_2}}. \tag{2}$$

Many studies are conducted, assuming that the operating source frequency f_0 is equal with both resonance frequencies of primary side and secondary side ($f_0 = f_1 = f_2$) [4]- [7].

However, when resonance frequency mismatch is taken into account, the above-mentioned condition is not true, and all the equations, simulation and experiment results in this paper are achieved, according to the resonance frequency mismatch condition ($f_0 \neq f_1 \neq f_2$).

In Fig. 1, output voltage V_2, input current I_1, output current I_2 are defined as shown in (3), (4) and (5) respectively, where V_1, R_1, R_2, R_L, ω_0, ω_1, ω_2 are input voltage, transmitter coil resistance, receiver coil resistance, load resistance, operating angular frequency, primary resonance angular frequency and secondary resonance angular frequency respectively.

Then, input and output power, P_{in} and P_{out} are calculated by (3,)(4) and (5), expressed as (6) and (7), respectively.

$$V_2 = R_L I_2 \tag{3}$$

$$I_1 = \frac{\left(R_2+R_L+j\omega_2 L_2\left(\frac{\omega_0}{\omega_2}-\frac{\omega_2}{\omega_0}\right)\right)V_1}{\left\{R_1+j\omega_1 L_1\left(\frac{\omega_0}{\omega_1}-\frac{\omega_1}{\omega_0}\right)\right\}\left\{R_2+R_L+j\omega_2 L_2\left(\frac{\omega_0}{\omega_2}-\frac{\omega_2}{\omega_0}\right)\right\}+\omega_0{}^2M^2} \tag{4}$$

$$I_2 = \frac{j\omega_0 M V_1}{\left\{R_1+j\omega_1 L_1\left(\frac{\omega_0}{\omega_1}-\frac{\omega_1}{\omega_0}\right)\right\}\left\{R_2+R_L+j\omega_2 L_2\left(\frac{\omega_0}{\omega_2}-\frac{\omega_2}{\omega_0}\right)\right\}+\omega_0{}^2M^2} \tag{5}$$

$$P_{in} = Re\left\{V_1\bar{I}_1\right\} = \frac{\left\{r_1(r_2+R_L)^2 + r_1\omega_2{}^2L_2{}^2\left(\frac{\omega_0}{\omega_2}-\frac{\omega_2}{\omega_0}\right)^2 + \omega_0{}^2M^2(r_2+R_L)\right\}V_1^2}{\left\{r_1(r_2+R_L) - \omega_1\omega_2L_1L_2\left(\frac{\omega_0}{\omega_1}-\frac{\omega_1}{\omega_0}\right)\left(\frac{\omega_0}{\omega_2}-\frac{\omega_2}{\omega_0}\right) + \omega_0{}^2M^2\right\}^2 + \left\{(r_2+R_L)\omega_1L_1\left(\frac{\omega_0}{\omega_1}-\frac{\omega_1}{\omega_0}\right) + r_1\omega_2L_2\left(\frac{\omega_0}{\omega_2}-\frac{\omega_2}{\omega_0}\right)\right\}^2} \tag{6}$$

$$P_{out} = Re\left\{V_2\left(\bar{I}_2\right)\right\} = \frac{\omega_0{}^2M^2R_LV_1^2}{\left\{r_1(r_2+R_L) - \omega_1\omega_2L_1L_2\left(\frac{\omega_0}{\omega_1}-\frac{\omega_1}{\omega_0}\right)\left(\frac{\omega_0}{\omega_2}-\frac{\omega_2}{\omega_0}\right) + \omega_0{}^2M^2\right\}^2 + \left\{(r_2+R_L)\omega_1L_1\left(\frac{\omega_0}{\omega_1}-\frac{\omega_1}{\omega_0}\right) + r_1\omega_2L_2\left(\frac{\omega_0}{\omega_2}-\frac{\omega_2}{\omega_0}\right)\right\}^2} \tag{7}$$

According to (6) and (7), input and output power are influenced by the operating angular frequency, primary and secondary resonance angular frequency. Moreover, the denominator of (6) and (7) are same and only the numerator is different, both numerators of (6) and (7) are included with operating source frequency and secondary resonance frequency. On the other hand, denominator is included with operating source frequency, primary and secondary resonance frequency. It can be concluded that the effectiveness of primary resonance frequency for both input and output power is same.

TABLE I
PARAMETERS OF TRANSMITTING AND RECEIVING COIL

Parameter	Transmitter	Receiver
Resisitance R_1, R_2	1.00 Ω	1.05 Ω
Inductance L_1, L_2	617 μH	617 μH
Coupling coefficient k	0.06	
Transmitting gap	300 mm	
Outer diameter	440 mm	
Number of turns	50 turns	

TABLE II
CAPACITENCES USED FOR EXPERIMENTAL VERIFICATIONS

f_1, f_2[kHz]	80.9	82.6	84.9	86.5	89.0
C_1, C_2[nF]	6.26	6.02	5.69	5.49	5.18

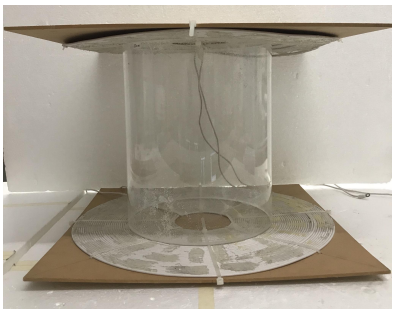

Fig. 2. Transmitting and receiving coil.

III. VERIFICATION(VALIDATION PARAMETERS)

The numerical analysis and experiment were conducted with the transmitting and receiving coil parameters shown in Tab. I. The Transmitting (primary side) and receiving (secondary side) coil in Fig. 2, are used for the experiment. Here, the load resistance is set as 10 Ω.

First, the resonance frequency range is selected from 81 kHz to 89 kHz, and the simulation is performed. For the experiment verification, only five different resonance frequencies (81 kHz, 83 kHz, 85 kHz, 87 kHz, 89 kHz) are chosen. The resonance frequency variation situation for the experiment, is created by changing the primary and secondary side capacitances as shown in Tab. II, those are calculated according to (1) and (2).

A. Theoretical Verifications

Fig. 3 and Fig. 4 shows the theoretical input and output power graphs respectively, against for operating source frequency are drawn for resonance frequency mismatch. The

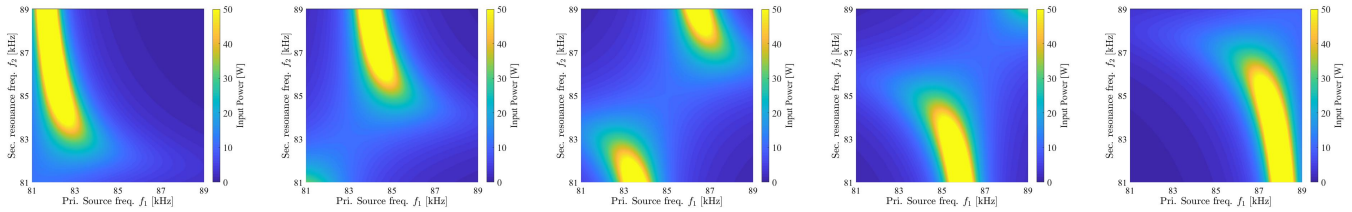

(a) f_0 = 81 kHz (b) f_0=83 kHz (c) f_0=85 kHz (d) f_0=87 kHz (e) f_0=89 kHz

Fig. 3. Theoretical results of input power. (a) f_0=81 kHz, (b) f_0=83 kHz, (c) f_0=85 kHz, (d) f_0=87 kHz, (e) f_0=89 kHz

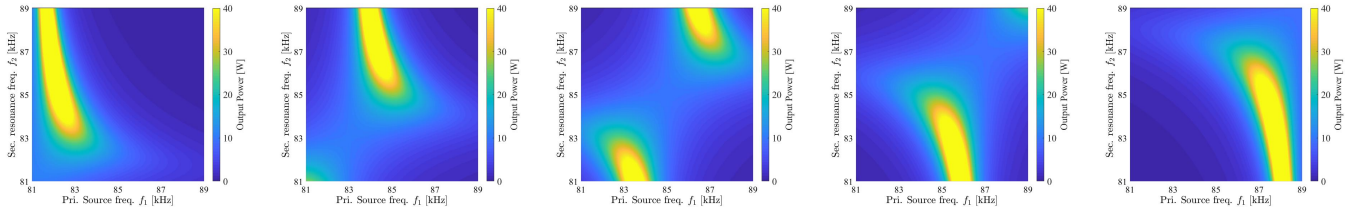

(a) f_0 = 81 kHz (b) f_0=83 kHz (c) f_0=85 kHz (d) f_0=87 kHz (e) f_0=89 kHz

Fig. 4. Theoretical results of output power. (a) f_0=81 kHz, (b) f_0=83 kHz, (c) f_0=85 kHz, (d) f_0=87 kHz, (e) f_0=89 kHz

horizontal axis is for primary resonance frequency variation and the vertical axis is for the secondary resonance frequency variation. The theoretical calculations are done at various operating source frequencies. It can be clearly seen from Fig. 3 and Fig. 4, the yellow color space represents the highest input and output power, moves both horizontally and vertically according to the primary and secondary side resonance frequency. Additionally, the tendency of output graph and input graph are same. However, as though the values output power are smaller than the input power values, which indicates the range of the color bar.

B. Experimental Verification

In the experiment, the Vector network analyzer (VNA)(E5061B ENA Series) was connected to port 1 and port 2 shown in Fig.1, and the input and output power were measured. The coils used for the measurements are shown in Fig. 2, and the parameters of the coils and capacitors are listed in Tab. I and Tab. II, respectively. The primary side capacitance C_1 is changed by replacing the capacitors; On the other hand, secondary side capacitance C_2 in Tab. I is varied by VNA. Load resistance of 10 Ω also set in VNA.

To compare the experiment results with the theoretical calculations, graphs are illustrated same as Fig. 3 and Fig. 4, and shown in Fig. 5 and Fig. 6 respectively, using the data obtained in experiment. Fig.5 and Fig. 6 are the experimental input and output power graphs respectively.

From Fig.5 and Fig. 6, It is clear that the highest input and output power is varied according to the primary and secondary resonance frequency. Theoretical results are indicated in Fig. 3 and Fig. 4, and experimental results are displayed in Fig.5 and Fig. 6 have the same behavior of the transmission power variation to resonance frequency mismatch.

C. Discussion

The tendency of input and output power graphs of Measurement result is almost given the similar result to the theoretical results for the WPT system with resonance frequency variation. As can be seen from both theoretical and measurement graphs of input and output power, larger input power which is nearly equal to the larger values are obtained when operating source frequency and primary resonance frequency is nearly equal. However, the shape of input power of measurement results has a little different with the theoretical results. This unstable condition may be caused by because of neglecting the equivalent series resistances (ESRs) values of capacitors and the components.

IV. Conclusion

This paper presented on the transmission power variation on the WPT system with resonance frequency mismatch. WPT circuit analysis here is performed to examine the influence of source frequency, and primary and secondary side resonance frequency to input and output power.

First, the theoretical formula of input and output power are expressed from the terms of operating frequency, primary and the secondary resonance frequency. With that theoretical formula, acquired the transmission power graph when the resonance frequency mismatch occur.

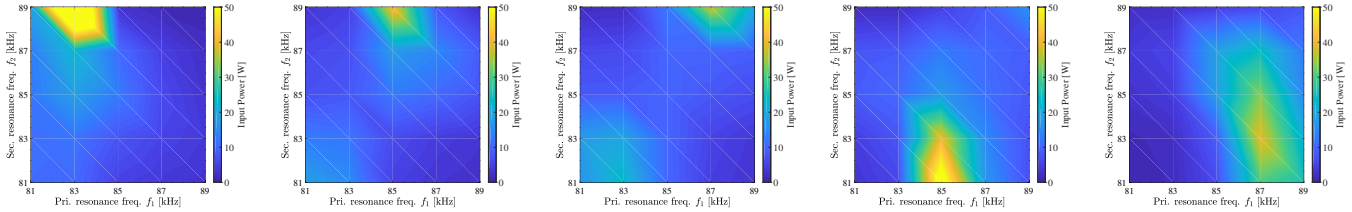

(a) f_0 = 81 kHz (b) f_0=83 kHz (c) f_0=85 kHz (d) f_0=87 kHz (e) f_0=89 kHz

Fig. 5. Experimental results of input power. (a) f_0=81 kHz, (b) f_0=83 kHz, (c) f_0=85 kHz, (d) f_0=87 kHz, (e) f_0=89 kHz

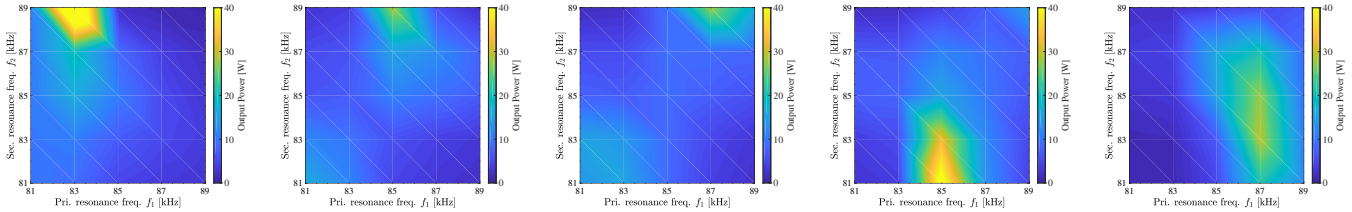

(a) f_0 = 81 kHz (b) f_0=83 kHz (c) f_0=85 kHz (d) f_0=87 kHz (e) f_0=89 kHz

Fig. 6. Experimental results of output power. (a) f_0=81 kHz, (b) f_0=83 kHz, (c) f_0=85 kHz, (d) f_0=87 kHz, (e) f_0=89 kHz

Finally, did the measurements to check the theoretical results for various resonance frequencies. It is confirmed that both input and output power is influenced by operating frequency, primary and the secondary resonance frequency when the resonance frequency mismatch occurs. In the future works, resistance of the capacitors the load resistance variation will be considered and transmission power maximization will be studied.

ACKNOWLEDGMENT

This work was partly supported by JSPS KAKENHI Grant Number 16J06942 and 17H04915.

REFERENCES

[1] Siqi Li, and Chunting Chris Mi, "Wireless Power Transfer for Electric Vehicle Applications," IEEE Journal of Emerging and Selected Topics in Power Electronics, Vol. 3, pp.4–17, March 2018.

[2] Chunting Chris Mi, Giuseppe Buja, Su Y. Choi, Chun T. Rim, "Modern Advances in Wireless Power Transfer Systems for Roadway Powered Electric Vehicles," IEEE Transactions on Industrial Electronics, Vol. 63, pp. 6533—6545, June 2016.

[3] Devendra Patil, Matthew K. McDonough, John M. Miller, Babak Fahimi, Poras T. Balsara, "Wireless Power Transfer for Vehicular Applications:Overview and Challenges," IEEE Transactions on Transportation Electrification, Vol. 4, pp. 3—37, December 2018.

[4] G. A. Covic, and J. T. Boys, "Inductive power transfer," Proceedings of the IEEE, Vol. 101, no. 6, pp. 1276–1289, June 2013.

[5] D. A. G. Pedder, A. D. Brown, and J. A. Skinner, "A contactless electrical energy transmission system," IEEE Transactions on Industrial Electronics, Vol. 46, pp. 23—30, February 1999.

[6] P. Sergeant and A. Van den Bossche, "Inductive coupler for contactless power transmission," IET Electric Power Applications, Vol. 2, pp. 1—7, February 2008.

[7] Zhongzheng Lin, Junhua Wang, Zhijian Fang, Meilin Hu, Changsong Cai, Junkun Zhang, "Coil Design and Measurements of Automotive Magnetic Resonant Wireless Charging System for High-Efficiency and Low Magnetic Field Leakage," IEEE Transactions on Microwave Theory and Techniques, Vol. 64, pp. 383–400, February 2016.

[8] Yao-Ching Hsieh, Zhong-Rong Lin, Ming-Cheng Chen, Hsin-Che Hsieh, Yu-Chen Liu, and Huang-Jen Chiu, "High-Efficiency Wireless Power Transfer System for Electric Vehicle Applications," IEEE Transactions on Circuits and Systems, Vol. 64, pp. 942—946, August 2017.

[9] Yiming Zhang, Ting Lu, Zhengming Zhao, Fanbo He, Kainan Chen, and Liqiang Yuan, "Selective Wireless Power Transfer to Multiple Loads Using Receivers of Different Resonant Frequencies," IEEE Transactions on Power Electronics, Vol. 30, pp. 6001—6005, August 2014.

[10] C.-S. Wang, G. Covic, and O. Stielau, "Power transfer capability and bifurcation phenomena of loosely coupled inductive power transfer systems," IEEE Transactions on Industrial Electronics, Vol. 51, pp. 148—157, February 2004.

[11] M. Budhia, G. A. Covic, and J. T. Boys, "Design and optimization of circular magnetic structures for lumped inductive power transfer systems," IEEE Trans. Power Electron, Vol. 26, pp. 3096—3108, November 2011.

[12] Takehiro Imura, and Yoichi Hori, "Maximizing Air Gap and Efficiency of Magnetic Resonant Coupling for Wireless Power Transfer Using Equivalent Circuit and Neumann Formula," IEEE Transactions on Power Electronics, Vol. 58, pp. 4746–4752, February 2011.

[13] Yeong H. Sohn, Bo H. Choi, Eun S. Lee, Gyu C. Lim, Gyu-Hyeong Cho, Chun T. Rim, "General Unified Analyses of Analyses of Two-Capacitor Inductive Power Transfer Systems: Equivalence of Current-Source SS and SP Compensations," IEEE Transactions on Power Electronics, Vol. 30, pp. 6030–6045, November 2015.

[14] Dukju Ahn, Seongmin Kim, Jungick Moon, and In-Kui Cho, "Wireless Power Transfer With Automatic Feedback Control of Load Resistance Transformation," IEEE Transactions on Power Electronics, Vol. 31, pp. 7876–7886, December 2015.

[15] A. Kurs, A. Karakis, R. Moffatt, J. D. Joannopoulos, P. Fisher, and M.Soljacic, "Wireless power transmission via strongly coupled magnetic resonances," Science, Vol. 317, pp. 83–86, July 2007.